

Article

Numerical Analysis of Stress Gradient and Traps Effects on Carbon Diffusion in AISI 316L during Low Temperature Gas Phase Carburization

Yawei Peng ^{1,2}, Jianming Gong ^{1,2,*}, Chaoming Chen ^{1,2}, Zhe Liu ^{1,2} and Yong Jiang ^{1,2}

¹ School of Mechanical and Power Engineering, Nanjing Tech University, No. 30 Puzhu South Road, Nanjing 211800, China; pengyw@njtech.edu.cn (Y.P.); 970153631@njtech.edu.cn (C.C.); liuzhe@njtech.edu.cn (Z.L.); jiangyong@njtech.edu.cn (Y.J.)

² Jiangsu Key Lab of Design and Manufacture of Extreme Pressure Equipment, No. 30 Puzhu South Road, Nanjing 211800, China

* Correspondence: gongjm@njtech.edu.cn; Tel.: +86-25-5813-9361

Received: 14 March 2018; Accepted: 21 March 2018; Published: 26 March 2018



Abstract: In order to elucidate the roles of the composition-induced stress gradient and the traps formed by chromium atoms in carbon diffusion in AISI 316L austenitic stainless steel during low temperature gas phase carburization, the carbon concentration-depth profiles were analyzed by a diffusion model considering the composition-induced stress gradient and the trapping effect. The results show that the carbon concentration-depth profiles calculated by this model show good agreement with the experimental results. The composition-induced compressive stress gradient can enhance the carbon diffusion but reduce the surface carbon concentration; these effects are not pronounced. Carbon atoms prefer to occupy the trap sites, and the detrapping activation energy ($Q_t = 33 \text{ kJ}\cdot\text{mol}^{-1}$) was deduced from fitting the experimental carbon concentration-depth profile. Furthermore, this applied diffusion model can be used to interpret the enhanced carbon diffusion in low temperature carburized AISI 316L.

Keywords: low temperature gas phase carburization; austenitic stainless steel; carbon diffusion; composition-induced stress gradient; trapping effect

1. Introduction

Owing to their favorable manufacturing performance and excellent corrosion resistance, austenitic stainless steels are widely used in many industrial environments, such as petrochemical, biomedical, food and nuclear industries [1]. However, their modest mechanical (low surface hardness and strength) and poor tribological (high friction and wear rate) properties [2,3] compared to other steels have restricted their applications in many engineering fields.

Thermochemical surface engineering, such as low temperature surface carburization ($<500 \text{ }^\circ\text{C}$), has been proven to be an effective means for improving the mechanical and tribological properties of austenitic stainless steel (Fe–Cr–Ni alloy); meanwhile, the corrosion resistance is maintained [4–8]. The origin of these improvements is that such that treatment can bring about a layer of expanded austenite, which essentially is a supersaturated solid solution of interstitial carbon atoms in austenite and without chromium carbide precipitation [9,10]. Investigating the diffusion behavior of carbon atoms in austenitic stainless steel during low temperature surface carburization may be conducive to figuring out the strengthening mechanism of low temperature surface carburization. By conducting a series of experiments on low temperature surface carburization of austenitic stainless steel under different in situ tensile stresses, Li et al. [11] found that the external applied tensile stress effectively thickened the layer of expanded austenite. Furthermore, in order to investigate the effect of external

compressive stress on the diffusion of carbon in a layer of expanded austenite, hydrostatic compressive stresses were applied through hot isostatic pressing to low temperature carburized 316 austenitic stainless steel [12]. The experimental results demonstrated that applied compressive stress can retard the fast diffusion process comparing to an unstressed state. It is well known that low temperature surface carburization of austenitic stainless steel can result in tremendous compressive stresses (GPa level) with graded distribution as a consequence of the lattice expansion associated with the dissolution of interstitial carbon [5,13–15]. It has been well established that the diffusion of atoms is dependent on the chemical potential gradient, and the stress gradient is one of the important factors determining the chemical potential gradient [16]. In addition, Cr has a stronger affinity than Fe and Ni for carbon atoms; this has been found in low temperature surface carburized AISI 316 through extended X-ray absorption fine structure (EXAFS) analysis [17], implying that short range ordering of carbon and chromium atoms occurs. In other words, chromium atoms can serve as traps of carbon atoms. Therefore, the composition-induced compressive stress gradient and the traps formed by chromium atoms are proposed to play roles in carbon diffusion in austenitic stainless steel during low temperature surface carburization. However, it is not easy to evaluate the effects on carbon diffusion through experimental methods.

Therefore, in this work, carbon diffusion in AISI 316L austenitic stainless steel during low temperature gas phase carburization was simulated with a diffusion model considering the composition-induced stress gradient and the traps formed by chromium atoms. The roles of the composition-induced stress gradient and the trapping effect in carbon diffusion were elucidated by numerical analysis.

2. Material and Experimental Procedures

Specimens of AISI 316L austenitic stainless steel with a composition (in at. %) of C 0.12, Cr 18.14, Ni 9.69, Mn 1.17, Si 0.95, Mo 1.16 and Fe balance were cut to $10 \times 10 \times 6 \text{ mm}^3$. All specimens were mechanically polished with 1200 grit SiC papers, followed by polished with $3.5 \mu\text{m}$ synthetic diamond grinding paste. Before carburization, the specimens were degreased and cleaned using acetone and alcohol in an ultrasonic bath.

To enable carbon atoms to diffuse into the substrate, the passivating Cr_2O_3 -rich layer from the surfaces of the specimens was activated in a gas mixture of HCl and N_2 for 4 h at $250 \text{ }^\circ\text{C}$. After surface activation, the specimens were carburized in a gas mixture of CO, H_2 and N_2 (proportion of volume flux 1:1.5:2.5) at $470 \text{ }^\circ\text{C}$ for 15 h and 30 h, respectively. More details of the low temperature gas phase carburization process used in this work have been described in previous works [18]. After carburization, the carburized specimens were cleaned by the ultrasonic method in ethanol, in order to remove the soot formed on the surfaces.

The carbon concentrations along the depth direction were determined by EPMA with wavelength-dispersive X-ray spectrometry (EPMA-1610, Shimadzu, Kyoto, Japan). For quantitative analysis, the obtained curve for the C $\text{K}\alpha$ line intensity was quantitatively evaluated in the terms of the local carbon concentration by comparison with the calibration curve that was obtained from a suite of Fe–C alloys with known compositions under equivalent experimental conditions.

3. Diffusion Model

3.1. Composition-Induced Stress Gradient

The present work assumes one-dimension diffusion of carbon in the depth direction, with reference to a flat surface. Based on thermodynamics, the driving force of diffusion is dependent on the chemical potential gradient. The chemical potential of carbon as a diffuser in the solid matrix can be defined as [16]:

$$\mu = \mu_0 + RT \ln(a_C) - V_C \sigma_h \quad (1)$$

where μ_0 is the chemical potential of carbon in the reference state, a_C is the activity of carbon, V_C is the partial molar volume of carbon; and σ_h is the hydrostatic stress (pressure), which is induced by incorporating the carbon into austenitic lattice.

Assuming that $a_C = f \cdot C$ (f is the activity coefficient of carbon) and V_C is a constant in this work, the diffusion flux (J) of carbon atoms in the depth direction under the gradient of chemical potential (μ) can be expressed as [19,20]:

$$J = -M \cdot C \cdot \frac{\partial \mu}{\partial x} = -D \left(\frac{\partial C}{\partial x} - \frac{V_C C}{RT} \frac{\partial \sigma_h}{\partial x} \right) \quad (2)$$

where C is the carbon concentration; M is the mobility of carbon; D is diffusion coefficient of carbon; R is the gas constant; and T is the carburizing temperature.

Thus, the diffusion equation in the presence of composition-induced stress gradient can be written as:

$$\frac{\partial C(x,t)}{\partial t} = D \frac{\partial^2 C(x,t)}{\partial x^2} - \frac{DV_C}{RT} \left[\frac{\partial C(x,t)}{\partial x} \frac{\partial \sigma_h(x,t)}{\partial x} + C(x,t) \frac{\partial^2 \sigma_h(x,t)}{\partial x^2} \right] \quad (3)$$

where x and t are the diffusion depth and carburizing time, respectively.

The stress states in the carburized layer are plane stress ($\sigma_{zz} = 0$) and a rotationally symmetric state ($\sigma_{xx} = \sigma_{yy} = \sigma_{//}$) [21]. Therefore, hydrostatic stress $\sigma_h = (\sigma_{xx} + \sigma_{yy} + \sigma_{zz})/3 = 2\sigma_{//}/3$. The compressive residual stress ($\sigma_{//}$) is dependent on the carbon concentration, and the σ_h can be simply expressed with the following relationship [21]:

$$\sigma_h = -\zeta(C(x,t) - C_0) \quad (4)$$

where ζ and C_0 are the proportionality constant and the carbon concentration in the untreated steel, respectively.

Substituting Equation (4) to Equation (3), the diffusion equation can be rewritten as:

$$\frac{\partial C(x,t)}{\partial t} = D \frac{\partial^2 C(x,t)}{\partial x^2} + \frac{DV_C}{RT} \zeta \left[\left(\frac{\partial C(x,t)}{\partial x} \right)^2 + C(x,t) \frac{\partial^2 C(x,t)}{\partial x^2} \right] \quad (5)$$

The second term on the right-hand side of the Equation (5) denotes the effect of composition-induced stress gradient on carbon diffusion. Subtracting the second term, the rest of the equation is the standard expression of Fick's second law.

3.2. Trapping Effect

As mentioned above, short-range ordering of chromium and carbon atoms was found in carbon expanded austenite [17]. Therefore, if the carbon atom is considered to be a diffuser, it may occupy two different octahedral interstitial sites in expanded austenitic lattice. One type of site is the diffusion sites, from which carbon atoms can easily escape due to the smaller activation barrier. Another type is the trap sites (associated with Cr) where carbon atoms have difficulty escaping due to the larger activation barrier. Based on the "trapping-detrapping" theory and diffusion models [22–24], the model used in this work should be based on the following assumption: (i) only one kind of trap formed by chromium atoms exists; (ii) each trap site can only trap one carbon atom; (iii) the trap concentration is constant in time and depth; (iv) the detrapping activation energy is irrespective of the fraction of the occupied traps; (v) a local equilibrium exists between carbon on the diffusion sites and carbon on the trap sites; and (vi) trapping and detrapping are diffusion-controlled and follow first-order kinetics. Furthermore, according to the EXAFS analysis of expanded austenite, the average coordination number of carbon around chromium is about 2.1 [17], which indicates that the trapping of one carbon atom requires three chromium atoms, i.e., each trap consists of three chromium atoms. On the basis of the EXAFS analysis

results and the assumption above, Figure 1 gives the schematic of the possible crystal structure of carbon expanded austenite and the diffusion paths of carbon in expanded austenite.

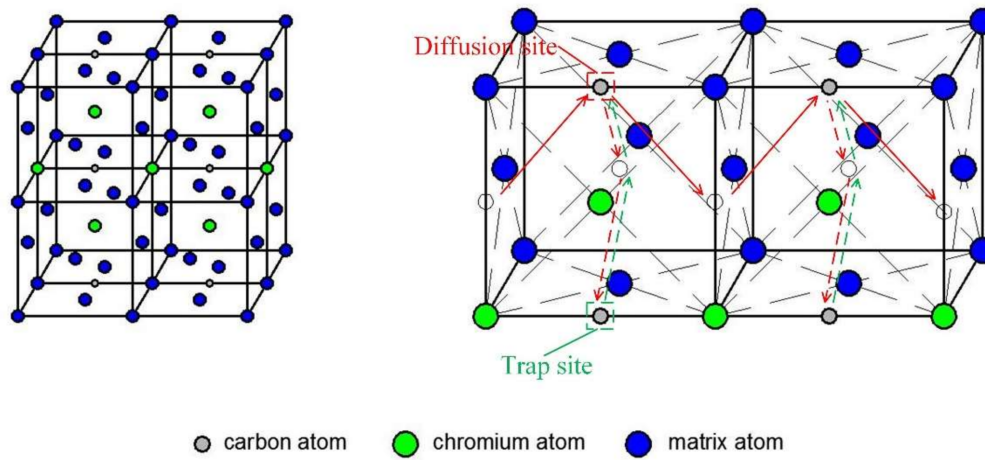


Figure 1. Schematic of the possible crystal structure of carbon expanded austenite and the diffusion paths of carbon in expanded austenite.

Therefore, considering the effect of the traps formed by chromium atoms on carbon diffusion, the diffusion equation (Equation (5)) can be rewritten as:

$$\frac{\partial C_d(x,t)}{\partial t} = D_d \frac{\partial^2 C_d(x,t)}{\partial x^2} + \frac{D_d V_C}{RT} \zeta \left[\left(\frac{\partial C_d(x,t)}{\partial x} \right)^2 + C_d(x,t) \frac{\partial^2 C_d(x,t)}{\partial x^2} \right] - S(x,t) \quad (6)$$

$$\frac{\partial C_t(x,t)}{\partial t} = S(x,t) = k_{d \rightarrow t} \cdot C_d(x,t) \left(1 - \frac{C_t(x,t)}{H_t / NA} \right) - k_{t \rightarrow d} \cdot C_t(x,t) \quad (7)$$

$$\frac{\partial C(x,t)}{\partial t} = \frac{\partial C_d(x,t)}{\partial t} + \frac{\partial C_t(x,t)}{\partial t} \quad (8)$$

where

$$D_d = D_0 e^{-\frac{Q_d}{RT}} \quad (9)$$

$$k_{d \rightarrow t} = 4\pi R_t H_t D_d \quad (10)$$

$$k_{t \rightarrow d} = 4\pi R_t H_0 D_d e^{-\frac{Q_t}{RT}} \quad (11)$$

where $S(x,t)$ denotes the trapping rate; $C(x,t)$ is the total carbon concentration; $C_d(x,t)$ and $C_t(x,t)$ are the carbon concentrations at the diffusion sites and the trap sites, respectively; D_d and D_0 are the carbon diffusivity at the diffusion sites and the pre-factor of diffusion, respectively; Q_d is the diffusion activation energy (taken as the diffusion activation energy of carbon in Fe–C austenite); Q_t is the detrapping activation energy; H_t is the trap concentration; H_0 is the host atom's concentration; R_t is the characteristic capture radius of trap site (taken as the lattice parameter); and NA is Avogadro's constant.

The first term and the second term in the expression of $S(x,t)$ describe the carbon atom trapping process and detrapping process, respectively.

3.3. Boundary Conditions

The surface concentration of the specimen during low temperature gas phase carburization depends on the balance of the arriving and leaving carbon fluxes. The flux of carbon atoms arriving at the surface (J_S) is given by [25]:

$$J_S = \beta \cdot (C_{eq} - C(0,t)) \quad (12)$$

where β is the mass transfer coefficient; C_{eq} is the carbon concentration in the solid-phase that would prevail if the imposed equilibrium was attained between carbon in the gas phase and carbon in solid solution, i.e., if the chemical potential of carbon in the gas phase and in solid solution were equal.

The boundary conditions are as follows:

$$\frac{\partial C_d(0,t)}{\partial t} = \frac{\beta \cdot (C_P - C_d(0,t) - C_t(0,t)) + D_d \left(1 + \frac{V_C \zeta}{RT} C_d(0,t)\right) \frac{\partial C}{\partial x}}{\Delta x} - S(0,t) \quad (13)$$

$$\frac{\partial C_t(0,t)}{\partial t} = S(0,t) = k_{d \rightarrow t} \cdot C_d(0,t) \left(1 - \frac{C_t(0,t)}{H_t/NA}\right) - k_{t \rightarrow d} \cdot C_t(0,t) \quad (14)$$

$$\frac{\partial C(0,t)}{\partial t} = \frac{\partial C_d(0,t)}{\partial t} + \frac{\partial C_t(0,t)}{\partial t} \quad (15)$$

where Δx is the increment of diffusion depth. In this work, the value of Δx is 1 μm .

The diffusion equations (Equations (6)–(8) and (12)–(15)) were solved by the finite difference approach (using MATLAB code). It should be noted that the value of the time increment (Δt) should be chosen to be sufficiently small enough in order to avoid instabilities or oscillations in the calculated results.

It should be noted that the diffusion model can only be used to describe carbon diffusion in austenitic stainless steel during low temperature gas phase carburization without chromium carbide precipitation.

4. Results and Discussion

To elucidate the roles of the composition-induced stress gradient and the traps formed by chromium atoms on carbon diffusion in austenite stainless steel during low temperature gas phase carburization, the experimental results were deduced from the diffusion equations (Equations (6)–(8) and (12)–(15)).

In order to solve the diffusion equations, all the model parameters must be determined. Besides the β and Q_t , other parameters can be determined from data in the literature: $R = 8.314 \text{ J} \cdot \text{mol}^{-1} \cdot \text{K}^{-1}$; $\zeta = 133 \text{ MPa} \cdot \text{at.} \%^{-1}$ [21]; $D_0 = 2 \times 10^{-5} \text{ m}^2 \cdot \text{s}^{-1}$ and $Q_d = 140 \text{ kJ} \cdot \text{mol}^{-1}$ [26]; $V_C = 4.2 \times 10^{-6} \text{ m}^3 \cdot \text{mol}^{-1}$ and $R_t = 0.36 \times 10^{-9} \text{ m}$ [27]; $H_0 = 4/(R_t)^3 = 8.27 \times 10^{28} \text{ m}^{-3}$ (the factor 4 arises because there are four host atoms per unit cell). Because each trap consists of three chromium atoms, $H_t = 0.1814 \cdot H_0/3 = 5 \times 10^{27} \text{ m}^{-3}$. The value of C_{eq} can be obtained by the following expression [28]:

$$\ln a_C = \ln\left(\frac{C}{1-C}\right) + \left(11.92 - \frac{6330\text{K}}{T}\right) \left(\frac{C}{1-C}\right) - 1.845 + \frac{5100\text{K}}{T} - \left(2.2 - \frac{7600\text{K}}{T}\right) C_{Ni} + \left(24.4 - \frac{38400\text{K}}{T}\right) C_{Cr} - \left(96.8 - \frac{84800\text{K}}{T}\right) C_{Cr}^2 \quad (16)$$

where C_i is the atomic fraction of an element. As mentioned above, there is soot on the surface of the carburized specimen; once the soot starts to form on the surface of the steel, the a_C will gradually decrease to one within the boundary layer of the gas flow, and the low temperature gas phase carburization treatment will actually be performed under a unit activity of carbon [29]. Therefore, the value of C_{eq} is 12.8 at. %.

The values of β and Q_t are obtained by fitting the experimental curve of the carbon concentration–depth profile of AISI 316L carburized at 470 °C for 15 h. The best fit is obtained at $\beta = 8 \times 10^{-10} \text{ m} \cdot \text{s}^{-1}$ and $Q_t = 33 \text{ kJ} \cdot \text{mol}^{-1}$.

Figure 2 shows the experimental and calculated carbon concentration–depth profiles of AISI 316L carburized at 470 °C for 15 h and 30 h. The carbon concentrations decrease monotonously with increasing depth and the concentration–depth profiles exhibit both convex and concave sections, which are obviously different from the error-function-like profiles (the standard analytic solution of Fick's second law). The calculated concentration–depth profiles show good agreement with the experimental results.

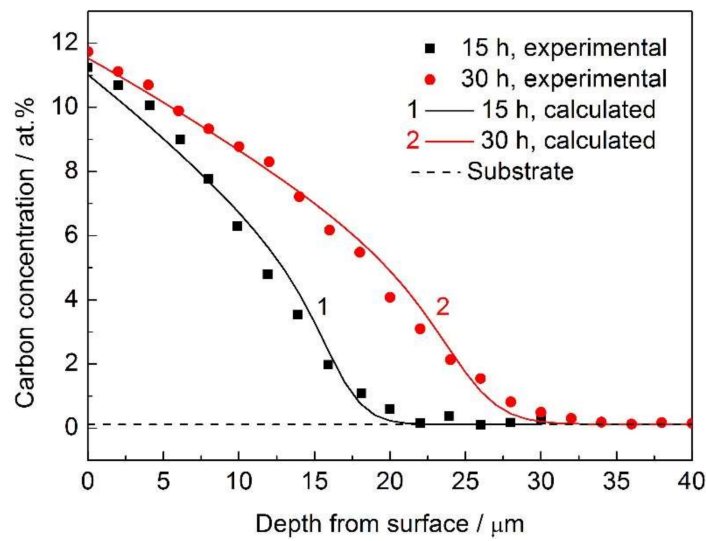


Figure 2. Experimental and calculated carbon concentration–depth profiles of AISI 316L carburized at 470 °C for 15 h and 30 h.

In order to further verify the applied model, another condition of the low temperature gas phase carburization process was tested with the diffusion equations (Equations (6)–(8) and (12)–(15)) with the same value of Q_t . The experimental conditions were the following: AISI 316L stainless steel (67.8 at. % Fe, 19.2 at. % Cr and 10.8 at. % Ni) was carburized in a gas mixture of CO, H₂ and N₂ at 723 K (450 °C). The carburization procedure included an initial carburization step of 4 h and a second carburization step of 38 h. More details and other needed model parameters can be found in reference [29]. Figure 3 shows the experimental and calculated carbon concentration–depth profiles of AISI 316L carburized at 450 °C for 42 h. It is very important to note that the calculated concentration–depth profile using the same value of Q_t shows good agreement with the experimental result obtained by Gu [29]. This proves that the diffusion model used in this work can explain the process of carbon diffusion in AISI 316L during low temperature gas phase carburization.

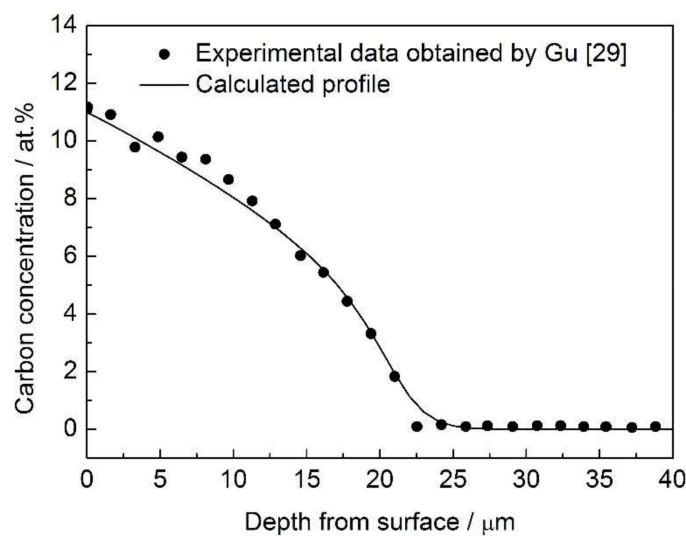


Figure 3. Experimental and calculated carbon concentration–depth profiles of AISI 316L carburized at 450 °C for 42 h.

In order to elucidate the effect of the composition-induced stress gradient on carbon diffusion in AISI 316L during low temperature gas phase carburization, residual stress–depth profiles of AISI 316L carburized at 470 °C for 30 h were calculated using different values of ξ , which are shown in Figure 4. It is noted that when the value of ξ is equal to zero, this implies that no composition-induced compressive residual stresses existed in the carburized AISI 316L. Actually, there are very large compressive residual stresses in the carburized AISI 316L; values can be in excess of 2 GPa at the surface and in gradient distribution after 30 h of low temperature gas phase carburization. Figure 5 gives the calculated carbon concentration–depth profiles of low temperature carburized AISI 316L using different values of ξ . It can be seen that due to the presence of the composition-induced compressive stress gradient, the diffusion of carbon in austenitic stainless steel during low temperature carburization is accelerated. However, this accelerating effect is not pronounced. Compared to the stress-induced nitrogen diffusion in the nitrogen expanded austenite modeled by Galdikas et al. [30,31], the role of the composition-induced compressive stress gradient in carbon diffusion is much weaker than in nitrogen diffusion. This may be ascribed to the difference in partial molar volume between carbon in expanded austenite and nitrogen in expanded austenite. The value of the partial molar volume of carbon in expanded austenite used in this work is only about one-tenth of that nitrogen in expanded austenite used by Galdikas et al. However, according to the research results of Christiansen et al. [27,32], the value of the partial molar volume of nitrogen in expanded austenite cannot be as large as that used in the works of Galdikas et al. [30,31]. Furthermore, the surface carbon concentration was lower due to the presence of the composition-induced compressive stress gradient. However, this effect was also not significant.

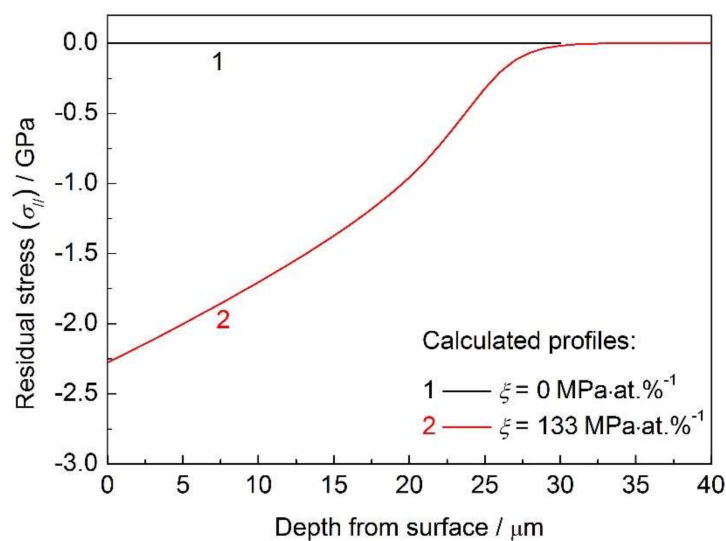


Figure 4. Calculated residual stress–depth profiles of AISI 316L carburized at 470 °C for 30 h using different value of ξ .

The influence of detrapping activation energy (Q_t) on carbon concentration–depth profiles is shown in Figure 6. As mentioned above, the best fit is obtained at $Q_t = 33 \text{ kJ}\cdot\text{mol}^{-1}$. It can be seen that when the detrapping activation energy decreases, implying that the effect of trapping has reduced, the diffusion depth of carbon increases. The diffusion process is more intensive when the detrapping activation energy is lower. When the detrapping activation energy increases, an abrupt drop in concentration occurs. This indicates that when the carbon concentration is relatively low, the diffusion process will be significantly affected by the traps.

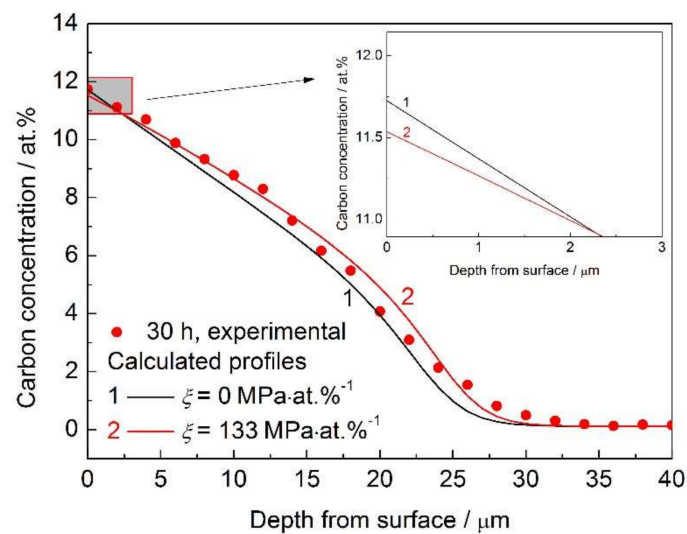


Figure 5. Calculated carbon concentration–depth profiles of AISI 316L carburized at 470 °C for 30 h using different values of ξ .

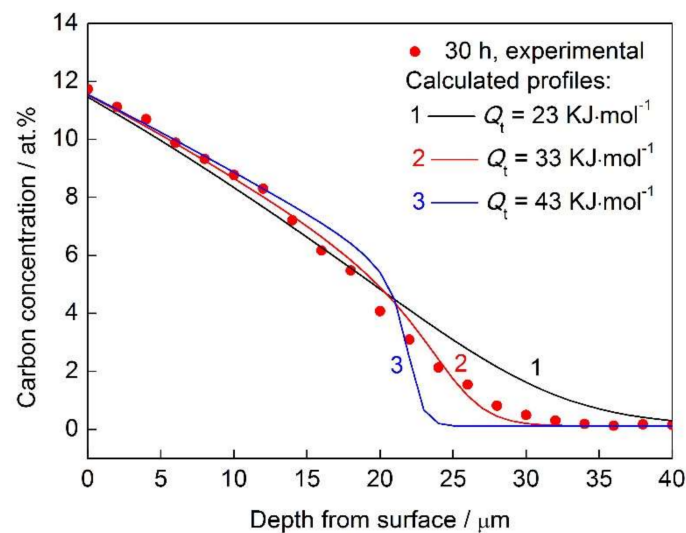


Figure 6. Influence of the detrapping activation energy (Q_t) on carbon concentration–depth profiles of AISI 316L carburized at 470 °C for 30 h.

Figure 7 gives the calculated concentration–depth profiles of carbon at the diffusion sites and the trap sites in AISI 316L carburized at 470 °C for different periods of time. The shapes of the calculated carbon concentration–depth profiles at the diffusion sites and at the trap sites are very different. At the diffusion sites, the carbon concentration–depth profiles exhibit typical diffusion shapes (error-function-like shape). The concentration–depth profiles of carbon at the trap sites exhibit a plateau at very beginning stage of the profiles; moreover, the plateau is more obvious with an increased carburizing time. This indicates that the carbon concentration at the trap sites of the outmost diffusion zone will be quickly saturated as time increases. The saturated concentration is little bit lower than the traps concentration (about 6.0 at. % in this work). This result is ascribed to the local equilibrium that exists between carbon at the diffusion sites and carbon at the trap sites.

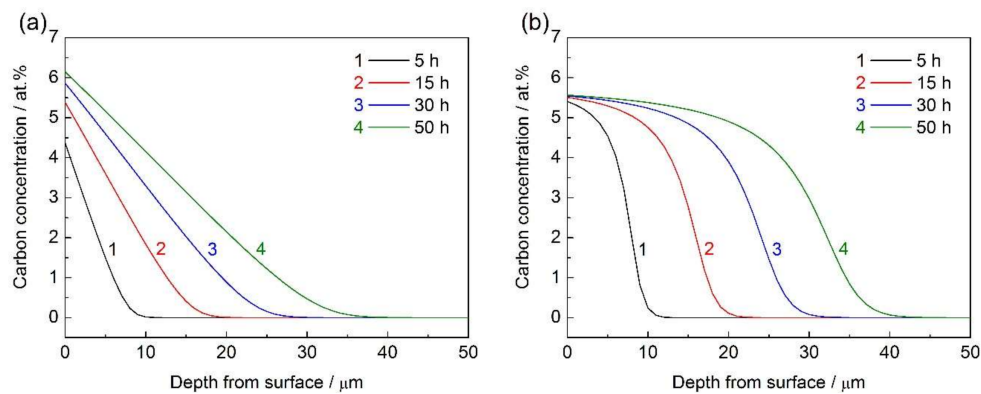


Figure 7. Calculated carbon concentration–depth profiles at different carburizing times: (a) at the diffusion sites; (b) at the trap sites.

Figure 8 gives the carbon concentration at the diffusion sites and the trap sites as a function of total carbon concentration. The carbon concentrations at the diffusion sites and the trap sites both increase with increasing total carbon concentration. Before the carbon concentration at the trap sites approaches saturation, the concentration of carbon at the trap sites is always larger than that of carbon at the diffusion sites. This indicates that the carbon atoms will give priority to occupying the trap sites during carbon diffusion in AISI 316L during low temperature gas phase carburization. Figure 9 gives the corresponding normalized carbon concentration growth rate of diffusion sites and trap sites as a function of total carbon concentration. With an increase in the total carbon concentration, the concentration growth rate of carbon at the trap sites decreases, while the concentration growth rate of carbon at the diffusion sites increases. Meanwhile, the carbon concentration growth rate at the trap sites is larger than that at diffusion sites when the total carbon concentration is relatively low. This is attributed to that the high affinity between carbon atoms and chromium atoms, which causes a large detrapping activation energy ($Q_t = 33 \text{ kJ}\cdot\text{mol}^{-1}$). The possibility of carbon atoms occupying the trap sites is bigger than that of diffusion sites; meanwhile, once the carbon atoms are trapped it is difficult for them to escape. Therefore, the carbon concentration growth rate of trap sites is larger than that of diffusion sites, and most of the carbon atoms are present at the trap sites when the total carbon concentration is relatively low. However, as the number of unoccupied trap sites becomes fewer and fewer, more carbon atoms can only occupy the diffusion sites. Therefore, the carbon concentration growth rate of diffusion sites is eventually larger than that of the trap sites.

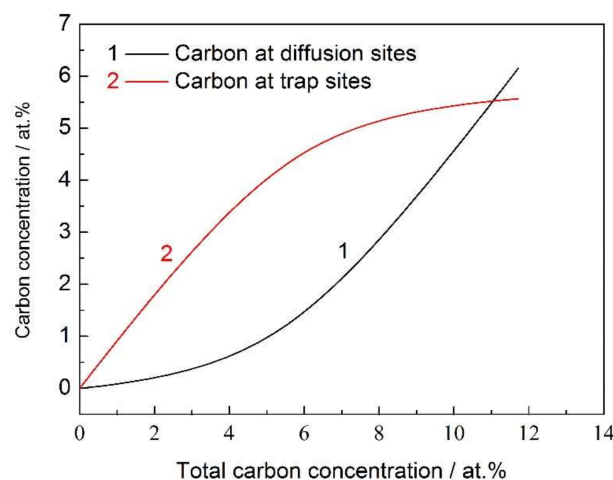


Figure 8. Carbon concentrations at the diffusion sites and the trap sites vs. total carbon concentration.

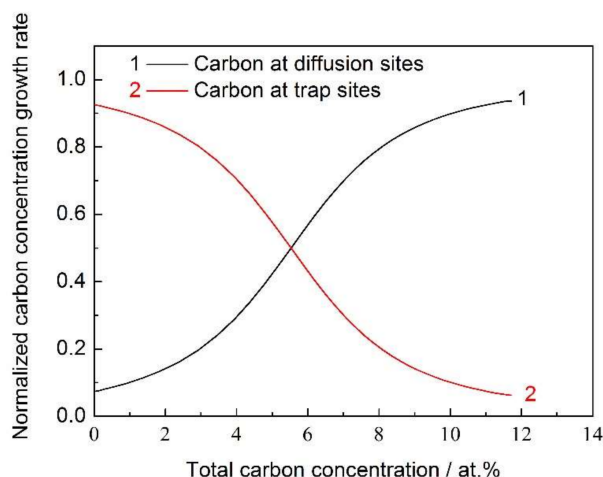


Figure 9. Normalized concentration growth rates of carbon at the diffusion sites and the trap sites vs. total carbon concentration.

The ratio between the carbon concentration at the diffusion sites and the trap sites as a function of total carbon concentration is shown in Figure 10. The ratio, C_d/C_t , increases as the total carbon concentration increases. It is easy to infer that the average value of the activation energy for carbon diffusion is very large when the total carbon concentration is relatively low because most of the carbon atoms are present at the trap sites. Thus, the carbon diffusion coefficient is very small. However, with an increase in the total carbon concentration, the ratio, C_d/C_t , increases. Accordingly, the average value of the activation energy for carbon diffusion will decrease and the diffusion coefficient will be enhanced. In particular, once the carbon concentration growth rate of diffusion sites is larger than that of trap sites, the diffusion coefficient will be significantly enhanced by the increasing total carbon concentration. Such an inference can plausibly be applied to explain the enhanced carbon diffusion in austenitic stainless steel carburized at low temperature, which was found by Ernst et al. [33].

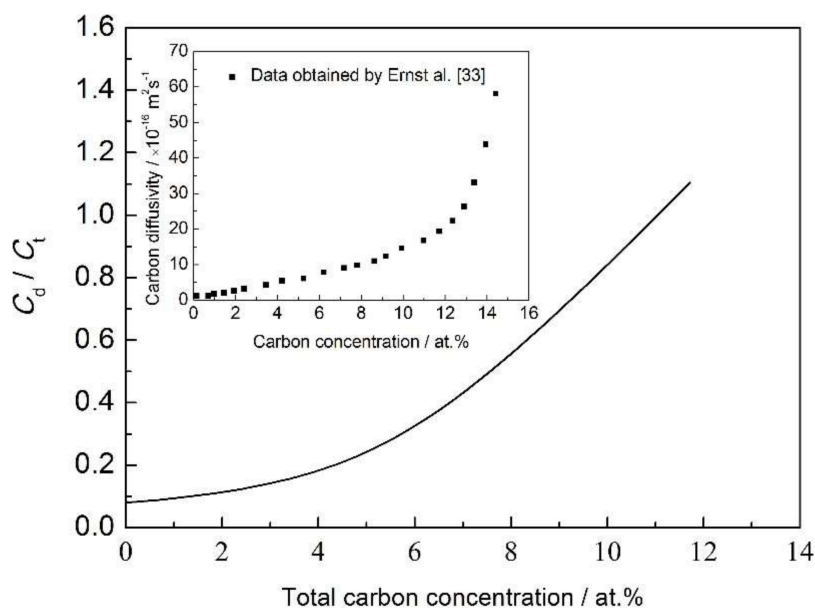


Figure 10. Ratio between carbon concentration at the diffusion sites (C_d) and carbon concentration at the trapping sites (C_t) as a function of total carbon concentration. Inset: carbon diffusion coefficient as a function of the total carbon concentration, as determined by Ernst et al. [33].

5. Conclusions

In this paper, the carbon diffusion in AISI 316L austenitic stainless steel during low temperature gas phase carburization was modeled. The roles of the composition-induced stress gradient and the traps formed by chromium atoms during carbon diffusion were revealed by numerical analysis. The main conclusions are as follows:

- The calculated carbon concentration–depth profiles based on the diffusion model considering the composition-induced stress gradient and the trapping effect by chromium were in good agreement with the experimental results.
- The composition-induced compressive stress gradient can enhance carbon diffusion in AISI 316L during low temperature gas phase carburization and reduce the surface carbon concentration. However, these effects are not remarkable.
- Carbon atoms prefer to occupy the trap sites, and the detrapping activation energy ($Q_t = 33 \text{ kJ}\cdot\text{mol}^{-1}$) was obtained from fitting the experimental data.

Acknowledgments: The work is supported by National Natural Science Foundation of China (No. 51475224), Natural Science Foundation of Jiangsu Higher Education Institutions of China (No. 14KJA470002) and Innovation Project for College Graduates of Jiangsu Province (No. KYZZ16_0234).

Author Contributions: Yawei Peng performed the calculations and wrote the manuscript; Jianming Gong supervised the findings of this work. Chaoming Chen, Zhe Liu and Yong Jiang assisted in the experiments and prepared the test specimens. All authors discussed the results and contributed to the final manuscript.

Conflicts of Interest: The authors declare no conflict of interest.

References

1. Davis, J.R. *Metals Handbook: Desk Edition*, 2nd ed.; ASM International Materials Park: Russell, OH, USA, 1998.
2. Hsu, K.L.; Ahn, T.M.; Rigney, D.A. Friction, wear and microstructure of unlubricated austenitic stainless steels. *Wear* **1980**, *60*, 13–37. [[CrossRef](#)]
3. Magee, J.H. Friction, lubrication and wear technology. In *ASM Handbook*; Blau, P.J., Ed.; ASM International Materials Park: Russell, OH, USA, 1998; Volume 18, pp. 710–724.
4. Jones, N.G.; Ward-Close, C.M.; Brown, P.M.; Dye, D. An evaluation of the tensile properties of a supersaturated carbon layer via in situ synchrotron diffraction. *Scr. Mater.* **2010**, *63*, 85–88. [[CrossRef](#)]
5. Michal, G.M.; Ernst, F.; Cao, Y.; Oba, F.; Agarwal, N.; Heuer, A.H. Carbon supersaturation due to paraequilibrium carburization: Stainless steels with greatly improved mechanical properties. *Metall. Mater. Trans. A* **2006**, *54*, 1597–1606. [[CrossRef](#)]
6. Christiansen, T.; Somers, M.A.J. Low temperature gaseous nitriding and carburising of stainless steel. *Surf. Eng.* **2005**, *21*, 445–455. [[CrossRef](#)]
7. Christiansen, T.L.; Somers, M.A.J. Low-temperature gaseous surface hardening of stainless steel: The current status. *Int. J. Mater. Res.* **2009**, *100*, 1361–1377. [[CrossRef](#)]
8. Qu, J.; Blau, P.J.; Jolly, B.C. Tribological properties of stainless steels treated by colossal carbon supersaturation. *Wear* **2007**, *263*, 719–726. [[CrossRef](#)]
9. Leyland, A.; Lewis, D.B.; Stevensom, P.R.; Matthews, A. Low temperature plasma diffusion treatment of stainless steels for improved wear resistance. *Surf. Coat. Technol.* **1993**, *62*, 608–617. [[CrossRef](#)]
10. Dong, H. S-phase surface engineering of Fe-Cr, Co-Cr and Ni-Cr alloys. *Int. Mater. Rev.* **2010**, *55*, 65–98. [[CrossRef](#)]
11. Li, W.; Li, X.; Dong, H. Effect of tensile stress on the formation of S-phase during low-temperature plasma carburizing of 316L foil. *Acta Mater.* **2011**, *59*, 5765–5774. [[CrossRef](#)]
12. Li, W.; Guo, W.; Zhu, X.; Jin, X.; Li, X.; Dong, H. The effect of applied compressive stress on the diffusion of carbon in carbon supersaturated S-phase layer. *Surf. Coat. Technol.* **2017**, *331*, 1–6. [[CrossRef](#)]
13. Christiansen, T.L.; Hummelshøj, T.S.; Somers, M.A.J. Expanded austenite crystallography and residual stress. *Surf. Eng.* **2010**, *26*, 242–247. [[CrossRef](#)]
14. Christiansen, T.L.; Somers, M.A.J. Stress and composition of carbon stabilized expanded austenite on stainless steel. *Metall. Mater. Trans. A* **2009**, *40*, 1791–1798. [[CrossRef](#)]

15. Rong, D.S.; Jiang, Y.; Gong, J.M. Residual stress in low temperature carburised layer of austenitic stainless steel. *Mater. Sci. Technol.* **2017**, *33*, 227–284. [[CrossRef](#)]
16. Li, C.M. Physical chemistry of some microstructural phenomena. *Metall. Mater. Trans. A* **1978**, *9*, 1353–1380.
17. Oddershede, J.; Christiansen, T.L.; Ståhl, K.; Somers, M.A.J. Extended X-ray absorption fine structure investigation of carbon stabilized expanded austenite and carbides in stainless steel AISI 316. *Steel Res. Int.* **2011**, *82*, 1248–1254. [[CrossRef](#)]
18. Peng, Y.W.; Gong, J.M.; Jiang, Y.; Fu, M.H.; Rong, D.S. The effect of plastic pre-strain on low-temperature surface carburization of AISI 304 austenitic stainless steel. *Surf. Coat. Technol.* **2016**, *304*, 16–22. [[CrossRef](#)]
19. Yang, F. Interaction between diffusion and chemical stresses. *Mater. Sci. Eng. A* **2005**, *409*, 153–159. [[CrossRef](#)]
20. Karabelchtchikova, O.; Sisson, R.D. Carbon diffusion in steels: A numerical analysis based on direct integration of the flux. *J. Phase Equilib. Diff.* **2006**, *27*, 598–604. [[CrossRef](#)]
21. Christiansen, T.; Somers, M.A.J. Avoiding ghost stress on reconstruction of stress- and composition-depth profiles from destructive X-ray diffraction depth profiling. *Mater. Sci. Eng. A* **2006**, *424*, 181–189. [[CrossRef](#)]
22. Parascandola, S.; Möller, W.; Williamson, D.L. The nitrogen transport in austenitic stainless steel at moderate temperatures. *Appl. Phys. Lett.* **2000**, *76*, 2194–2196. [[CrossRef](#)]
23. Martinavičius, A.; Abrasonis, G.; Möller, W. Influence of crystal orientation and ion bombardment on the nitrogen diffusivity in single-crystalline austenitic stainless steel. *J. Appl. Phys.* **2011**, *110*, 259. [[CrossRef](#)]
24. Moskalioviene, T.; Galdikas, A.; Rivière, J.P.; Pichon, L. Modeling of nitrogen penetration in polycrystalline AISI 316L austenitic stainless steel during plasma nitriding. *Surf. Coat. Technol.* **2011**, *205*, 3301–3306. [[CrossRef](#)]
25. Karabelchtchikova, O. Fundamentals of Mass Transfer in Gas Carburizing. Ph.D. Thesis, Worcester Polytechnic Institute, Worcester, MA, USA, November 2007.
26. Hu, G.X.; Cai, X.; Rong, Y.H. *Fundament of Materials Science*, 3rd ed.; Shanghai Jiao Tong University Press: Shanghai, China, 2010; ISBN 9787313024800.
27. Hummelshøj, T.S.; Christiansen, T.L.; Somers, M.A.J. Lattice expansion of carbon-stabilized expanded austenite. *Scr. Mater.* **2010**, *63*, 761–763. [[CrossRef](#)]
28. Natesan, K.; Kassner, T.F. Thermodynamics of carbon in nickel, iron-nickel and iron-chromium-nickel alloys. *Metall. Trans.* **1973**, *4*, 2557–2566. [[CrossRef](#)]
29. Gu, X. Numerical Simulations of Concentration-Depth Profiles of Carbon and Nitrogen in Austenitic Stainless Steel Based upon Highly Concentration Dependent Diffusivities. Ph.D. Thesis, Case Western Reserve University, Cleveland, OH, USA, May 2011.
30. Galdikas, A.; Moskalioviene, T. Stress induced nitrogen diffusion during nitriding of austenitic stainless steel. *Comp. Mater. Sci.* **2010**, *50*, 796–799. [[CrossRef](#)]
31. Galdikas, A.; Moskalioviene, T. Modeling of stress induced nitrogen diffusion in nitrided stainless steel. *Surf. Coat. Technol.* **2011**, *205*, 3742–3746. [[CrossRef](#)]
32. Christiansen, T.; Somers, M.A.J. Controlled dissolution of colossal quantities of nitrogen in stainless steel. *Metall. Mater. Trans. A* **2006**, *37*, 675–682. [[CrossRef](#)]
33. Ernst, F.; Avishai, A.; Kahn, H.; Gu, X.; Michal, G.M.; Heuer, A.H. Enhanced carbon diffusion in austenitic stainless steel carburized at low temperature. *Metall. Mater. Trans. A* **2009**, *40*, 1768–1780.

